ijmc

# Effect of Electric Field on PD Activityand Damage into Solid Dielectric Materials

Alireza Ganjovi[1]

*Photonics research institute, Institute of Science and High Technology and Environmental Sciences, Graduate University of Advanced Technology, Kerman, Iran.*

**Abstract**. In this paper, the effect of applied electric field on the damagedue to partial discharges activity into the surroundings dielectrics of a narrow channel encapsulated within the volume of a dielectric materialis evaluated using a kinetic model based on Particle in Cell - Monte Carlo Collision (PIC-MCC) model. After application of an electric field across a dielectric material which contains a narrow channel,repeated ionization processstarts in the gaseous medium of narrow channel. Charged particles, especially electrons, gain energy from the electric field across narrow channel and cause damage into dielectric surfaces of narrow channel on impact.The dependence of the electron energy distribution function (EEDF) on the applied electric field is studied. It isseen that, during PD activity within narrow channel,the damage to the surrounding dielectrics and consequently the surface conductivity increases. These estimationsare performed based on the number of C-H bond-scissions produced by the impacting electrons of a single PD pulse. Based on this technique, the consequent damage into the solid dielectric and the time required to increase surface conductivity is computed.The formation of acid molecules due to interaction of PD pulse with polymer surface in presence of air and humidity causes changes in the surface conductivity of the surrounding dielectrics of the narrow channels.

**Index to information contained in this paper**

*Corresponding author. Email:ganjovi@icst.ac.ir; alirezaganjovi@yahoo.com

## 1. Introduction

**G**enerally, high voltage apparatus under operating conditions are subjected todamaging effects of activity of partial discharges into surrounding dielectrics of the existing narrow channel encapsulated within the volume of a dielectric material.A PD pulse generates energetic charged particles and photonsand they transfer sufficient energy to the polymer surfaces to break covalent bonds and form radicals. Usually, the polymer radicals react rapidly with oxygen [20].

The droplets of glycolic and formic acid as degradation products are identified by Hudon et al. They form initially on the surfaces of surrounding dielectrics of narrow-channel [20]. These acid molecules are much more conductive than the epoxy resin matrix, which is responsible for a rapid increase in surface conductivity [21, 22]. Moreover, while spark-type PD pulses occur when the surface conductivity is very low, glow discharges are observed after the surface becomes more conductive [25]. An increase in surface conductivity not long after the PD process was initiated in polyethylene [35].

The changes in discharge behavior associated with changes in the electrical characteristics of solid dielectric materials during the course of the discharge are investigated by Ishida et al. [25]. Some other authors also detected the formation of acid molecules due to interaction of discharge with polymer surfaces [10, 18, 32, 33].

Rogers showed that 'self-extinction' of pulsating PD in a dielectric cavity can be attributed to a discharge-induced increase in the conductivity of the cavity walls [40]. The conclusions by Tanaka etal.show that the nature of discharges is influenced by physical properties of the inner-surface of a cavity [44].They resulted that the discharge itselfcauses any change in electrical conductivity of the surface. Auckland et al. [2] observed that the charge on channel walls influenced the characteristics of breakdown in an artificial channel.

The proposed aging and life model based on electro-thermal degradation processes and space charge effects by Serra et al. [42] was useful to study the damage originating from microscopic defects such as micro-voids. They considered the degradation within a polyethylene-based material as a bond-breaking process due to impact of hot electrons, with the damage accumulating with time at void-polymer interfaces.

The dependence of insulation time to failure on applied field, temperature and cavity size were studied quantitatively [18, 30-31]. A two dimensional fluid model proposed by Novak et al. [37]. They studied the effect of charge produced by ionization on the surrounding solid insulation. They estimated the average kinetic energy of the electrons

and ions to be approximately 10eV and 0.6eV, respectively.

Although the aging and life model developed by Serra et al. [42] gives an estimate of damage on cavity walls due to hot electrons, one of its major drawbacks lies in that the electric field within the void is assumed constant. Consequently the spatial distribution of charged particles (electrons) within the void is neglected.

The electron energy distribution functions (EEDF) are assumed to be space-independent. Moreover, the model is one-dimensional, so that the interaction of charged particles with the side-walls of the cavity is not considered. Novak et al. [37] used a fluid model, where transport and swarm parameters such as ionization and attachment coefficient, velocities, EDF of electrons and ions, etc must be known in advance. It therefore becomes obvious that a relatively assumption-free model capable of estimating effect of PD pulse on channel walls in very narrow channels in terms of damage and increase in surface conductivity through particle bombardment of surrounding dielectrics, is required [19, 27, 39, 46-48].

In this paper, a two dimensional kinetic model based on PIC-MCC technique is extended to study the effect applied electric field on the PD pulse activityand the consequent damage into solid dielectric material and time required to increase surface conductivity of dielectric surrounding the dielectric narrow channel. The electron energy distribution function (EEDF) provides a more detailed description of the partial discharges on the dielectric anode and side walls. So, the dependence of the EEDFon the applied electric field is examined.
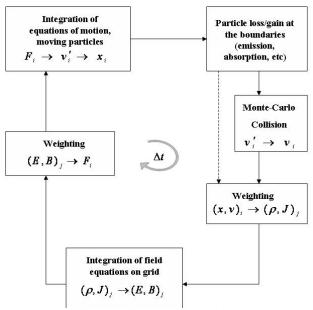


Figure 1: Schematic representation of the computation sequence for Particle in Cell-Monte Carlo (PIC-MCC) method.

## 2. Computational Method for PD within Narrow Channel

In the PIC scheme, particles are defined in a continuum position and velocity space. Field values are defined at discrete locations in space. Particle and field values are advanced sequentially in time, starting from initial conditions. The particle equations of motion are solved at every time step, using field values interpolated from the discrete grid to particle locations. The force on every particle is computed by interpolation of the field values from the grid position to the given particle positions. The position and velocities of each particle is next updated based on the solution of the classical equation of motion [33]. Next, particle boundary conditions are applied. For modeling collisions, the Monte Carlo collision (MCC) scheme is applied [47]. Source terms for the field equations are accumulated from the particle locations to the grid locations. The field values are then advanced by one time-step, and the time loop starts again (figure 1).

In the PIC-MCC scheme, each super-particle, representative of one or a much larger number of real particles, is designated in continuum space by its position and velocity. Initially, a Maxwellian distribution is assumed for electrons and ions. Further, the particles are uniformly distributed in the gap space. Particle boundary conditions such as absorption and emission are used to account for the relation between the discharge current in the gap and the current in the external circuit. When an electron or ion passes from the discharge into an end wall, it adds to the wall charge and is deleted from the list of active particles [27]. Additionally, secondary emissions occur when a charged particle impacts a surface (metallic or dielectric) causing ejection of electrons from the surface.

In the current work, the gas within the cavity is assumed to be air at atmospheric pressure. Therefore, photo-emission at the cathode is likely to be the dominant secondary emission process, rather than electron emission from cathode or anode due to ion or electron bombardment. However, all of the above processes have been accounted for in the model. After emission of a new electron, its energy is also assigned from an assumed Maxwell-Boltzmann distribution. The interaction of charged particles with neutral atoms and molecules, and other collisional processes are included by using a Monte Carlo Collision technique [8]. Three main charged particle species, viz. electrons, positive ions and negative ions have been considered. The major electron-neutral molecule impact reactions included are (i) elastic, (ii) excitation, (iii) ionization (including all important ionization reactions) and (iv) electron attachment. Related cross sectional values are extracted from experimental data available in the literature [39]. Integral cross section values for electron interaction in dry air have been determined from its molecular

constituents by assuming a target composition of 78.09%$N_2$and 21.19%$O_2$ [41]. Only elastic and charge transfer collisions between ions and neutrals are considered. Because ion-molecule cross sections are not readily available, a constant cross section $(10^{-20}m^2)$ has been assumed based on a hard-sphere collision model [51].
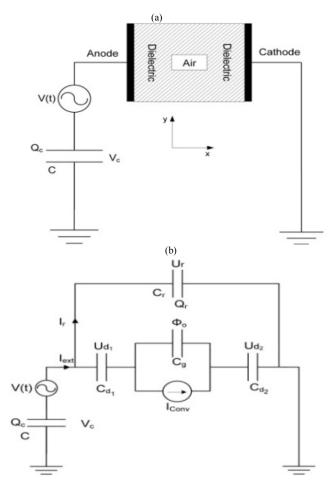


Figure 2: (a) The geometry of two dimensional dielectric-dielectric narrow channel; the external circuit consists of a voltage source and a blocking capacitor which stops the flow of average current, (b) the corresponding equivalent circuit.

A significant contribution of this work is that the discharge within the cavity is simulated in conjunction with an external circuit comprising of a voltage source, and a blocking capacitor that stops the flow of any average current. The coupling between the charge flow within the micro-cavity and the external current is obtained via the parallel-plane electrodes, which may be metallic or dielectric, depending on the location of the discharge site.

The potentials and fields are obtained using Poisson's equation:

$$\nabla \cdot \varepsilon_0 \nabla \Phi(x,t) = \rho(x,t) \quad (1)$$

The potential ($\Phi$) can be separated as follows [8, 28, 29]:

$$\Phi = \Phi_P + \sum_{Boundaries} \Phi_L \quad (2)$$

where $\Phi_P$ and $\Phi_L$ represent the Poisson and Laplacian parts of electrical potential ($\Phi$).

Therefore, the field may be described by the combination of the following equations:

$$\nabla \cdot \varepsilon_0 \nabla \Phi_P = -\rho \quad (3)$$

$$\nabla \cdot \varepsilon_0 \nabla \Phi_{Li} = 0 \quad (4)$$

The boundary condition for equation (3) is $\Phi=0$ on all boundaries as the Poisson field is solely due to charge in the medium. For each boundary with a Dirichlet condition, equation (4) is solved for $\Phi_i=0$ on the equipotential surface, and $\Phi=0$ elsewhere which gives us $\Phi_{Li}$(the potential due to the i$^{th}$Laplacian field). $\Phi_L$ is obtained by the superposition of all the Laplacian fields. Neumann boundary conditions are included through $\Phi_P=0$. This method neglects charges induced by a driven electrode on other boundaries which are connected to an external circuit. It is also possible to solve the field Poisson equation with boundaries and circuits [8, 33, 49].

In this work, identical cavities, as might occur at discharge sites, with two different electrode configurations have thus been considered. These are the two generic cases described below. The model is two-dimensional with Neumann boundary conditions on the side-walls. Dirichlet boundary conditions (potential drop specified) are assumed on the electrodes.

A narrow channel bounded by dielectrics on both sides is depicted in Figure 2(a). The equivalent circuit of this configuration is shown in Figure 2(b), where $C_g$, $C_{d1}$, $C_{d2}$ and $C_r$ represent the equivalent capacitances of the gap, the dielectric layers and dielectric material parallel to the micro-channel, respectively. The discharge current may be represented by $I_{conv}$. Using KCL, it is possible to obtain the following relations [34, 44, 48]:

$$C_d \frac{dU_d}{dt} = I_{ext} - I_r \quad (5)$$

$$A \frac{d\sigma_s}{dt} = I_{ext} - I_r + AJ_{conv} \quad (6)$$

$$V_c = V(t) - 2U_d - \phi_0 \quad (7)$$

$$U_r = 2U_d + \phi_0 \quad (8)$$

where$I_{ext}$ and $\sigma_T$ are the total external current and charge on the dielectric surface. $I_r$ is the leakage current flowing in the bulk of dielectric material parallel to the narrow channel. By

combining the above equations, equation (27) in ref. [48] may be rewritten as follows:

$$\phi_0^t = (\sigma_{s_T}^{t-1} + \frac{1}{A}(\alpha CV(t) - \alpha Q_c^{t-1} + \alpha Q_r^{t-1} - 2\alpha(C + C_r)U_d^{t-1} + Q_{Conv}^t) + \frac{\Delta x}{2}\sum_{j=0}^{j=N}\rho_{0j} + \frac{\varepsilon}{\Delta x}\sum_{j=0}^{j=N}\phi_{1j})(\frac{\varepsilon}{\Delta x}N + \alpha(C + C_r)/A)^{-1}$$

(9)

where α=(1+2(C+C$_r$)/C$_d$)$^{-1}$. σ$_T$, A, C, V(t), Q$_c$, Q$_r$, Q$_{conv}$, ρ, φ$_{ij}$ and N$_j$ are respectively the total surface charge density on the electrodes at a given time 't', cross sectional area of electrode, capacitance of blocking capacitor, driving voltage, charge in the external circuit, charge in the bulk of dielectric material parallel to the narrow channel, charge convection due to discharge, space charge density, the electric potential at each grid point and the number of grid divisions along the y-axis. The derivation of equation (5) is presented in appendix 1.

## 3. Computation of Damage and Change in Surface Conductivity

In this section, we describe the methodology adopted for computation of damage. Electrons produced within a narrow channel during a PD pulse, are accelerated by the applied field and reach the dielectric electrode with high energies. Additionally, during transit, they may also strike the dielectric side-walls of the narrow channel. The trajectory of each electron participating in the discharge is followed until it strikes a dielectric surface (wall or anode). The energy distribution functions (EEDF) of the electrons at the dielectric anode, and at the dielectric side walls are computed. The dielectric is assumed to be epoxy resin, which has a preponderance of C-H and C-C bonds. The impact of the electrons on the dielectric may cause chemical degradation of the material. In this work, the damage is assessed solely in terms of the amount of polymer that undergoes C-H bond scission through electron impact. The dissociative electron attachment (DEA) or ionization of C-H bonds requires approximately 8eV [42]. The damage due to each electron impact is computed in the following manner. Table I shows the electrons divided into a number of groups. Of the groups outlined in Table I, the first group (g$_1$) contains electrons with energy less than 8eV (ε< 8eV). These are cold electrons, and are considered to be irrelevant from the point of damage accumulation, as they are unable to produce irreversible degradation [42]. Electrons belonging to the remaining groups have energies beyond 8eV, and are capable of causing bond-scission. In every scattering event, an electron loses approximately 8eV, and shares the remaining energy equally with a secondary electron produced by impact ionization. Each electron is allowed to go through several scattering processes until its energy falls below 8eV. Thus, all high energy electrons ultimately cool to energy values smaller than 8eV [18, 30-31, 40, 42].

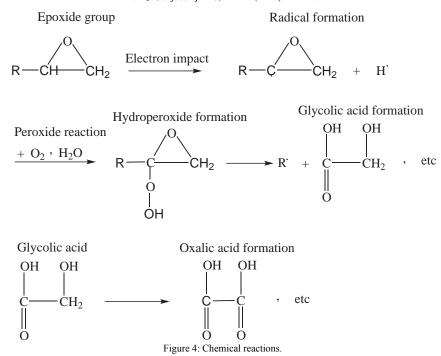**TABLE I: THE NUMBER OF C-H BONDS SCISSIONS DUE TO ONE ELECTRON ($N_k$) FOR DIFFERENT ELECTRON ENERGY GROUPS.**

| Group | Electron energy domain | $N_k$ |
|-------|------------------------|-------|
| $g_1$ | $\varepsilon < 8eV$ | 0 |
| $g_2$ | $8eV \leq \varepsilon < 24eV$ | 1 |
| $g_3$ | $24eV \leq \varepsilon < 56eV$ | 3 |
| $g_4$ | $56eV \leq \varepsilon < 120eV$ | 7 |
| $g_5$ | $120eV \leq \varepsilon < 248eV$ | 15 |
| $g_6$ | $248eV \leq \varepsilon < 504eV$ | 31 |

Electrons belonging to group $g_2$, possess energies between 8eV and 24eV. This energy is sufficient to cause only one C-H bond-break, as the excess energy when shared between a primary and a secondary, produces cold electrons. The subsequent groups are based on the number of C-H bond-scissions that electrons belonging to the respective groups can cause before they thermalize. The thermalization process is very fast, i.e. of PD pulse duration (<50ps) [30, 42]. The number of C-H bond-scissions due to any electron in group $g_k$, may thus be expressed as ($N_k = 2^{k-1} - 1$). The number of C-H bonds which can be broken by one PD pulse ($n_{CH}$) is calculated as the sum of bond-breaks by all electrons belonging to groups $g_2$ to $g_6$ (normally electrons with higher energies than those pertaining to $g_6$ are not produced in a single PD event), as shown below:

$$n_{CH} = \sum_{k=2}^{6} (2^{k-1} - 1) N_{gk} \qquad (10)$$

where $N_{gk}$ is the number of electrons in the respective group ($g_2$ to $g_6$).



Figure 3: Molecular formulae of DGEBA monomer.

Epoxide group                        Radical formation

Electron impact

Peroxide reaction      Hydroperoxide formation      Glycolic acid formation

$+ O_2 , H_2O$

Glycolic acid              Oxalic acid formation

Figure 4: Chemical reactions.

Diglycidyl ether of bisphenol-A (DGEBA) is a typical commercial epoxy resin and is chosen, in this work, as the base material to illustrate the mechanism of damage computation. Figure 3 shows the molecular structure of DGEBA. Thus, each DGEBA monomer has 24 C-H bonds. The radius of a DGEBA monomer is approximately $R(\approx 13.28 A^0)$ [45], and its cross-sectional area is approximately $A_{DGEBA}=5.546\times10^{-18}m^2$. The cross sectional area of the dielectric anode is $A_{anode}=L_y\times L_z$ and the area of each side wall is $A_{side-walls}=L_x\times L_z$. The number of DGEBA monomers on the surface of the dielectric anode and cathode is thus approximately $(N_{DGEBA})_{anode}= (N_{DGEBA})_{cathode} = A_{anode}/A_{DGEBA}$, and that on the surface of side wall is $(N_{DGEBA})_{side-walls} = A_{side-walls}/A_{DGEBA}$. The areas degraded from the dielectric anode and side-walls due to one PD pulse are estimated as follows:

$$\delta A_{anode} =\left(\frac{n_{CH}}{24\times N_{DGEBA}}\right)_{anode} A_{anode} \qquad (11)$$

$$\delta A_{side-wall} =\left(\frac{n_{CH}}{24\times N_{DGEBA}}\right)_{side-wall} A_{side-wall}$$

Chemical analysis of the deteriorated region in a micro-channel using microanalysis [43] showed that as a result of the intense spark discharge activity, complex chemical reactions take place between the plasma and the polymer surface. Energetic electrons (> 4.3eV) from the discharge transfer sufficient energy to the polymer surface to break

251

covalent bonds (C-H bonds), thus giving rise to radical formation from epoxide groups in DGEBA monomer. It is commonly assumed in the literature [10-14, 20-25, 50] that surface oxidation during discharge treatment is via a free radical process which is presented in figure 4.

The water may either be present as trapped moisture in the epoxy matrix, or it may originate as one of the degradation by-products. The first few steps probably occur during the large pulse discharge (spark-type) regime [20]. The formation of the oxalic acid crystals, constitutes the final step of the reaction sequence, and is predominantly manifest during the pseudo-glow and glow discharge regimes. The results of Hudon et al for evaluation of surface conductivity with time suggest that droplets (formed in presence of spark discharges) have a more pronounced effect on surface conductivity than the crystals formed under glow discharge conditions [20-25]. Morshuis et al. showed that if one of the constituents H, C or O was absent, no droplet appeared [35, 36].

The breaking of C-H bonds due to electrons in DGEBA monomer requires at least 4.3eV. Based on chemical reactions presented in figure 3, we assume that each epoxide ring is responsible for formation of only one acid molecule. So, every DGEBA monomer containing two epoxide rings would produce only two acid molecules (figure 3). We further assume for the sake of convenience, that the cross section of each acid molecule is equal to that of one epoxide ring. The process of C-H bond breaking in DGEBA monomer is assumed to be probabilistic event. The probability of a C-H bond break is calculated as:

$$P = 2(\pi r^2 / \pi R^2)/3,  \qquad (12)$$

where $r(\approx 2A^0)$ and R are the radius of epoxide ring and DGEBA monomer, the coefficient '3' in the denominator owes its existence to three C-H bond in every epoxide ring. The number of acid molecules ($N_a$) which can be formed due to one PD pulse is obtained as $(N_a)_{anode}= P \times (N_{CH})_{anode}$ and $(N_a)_{side-walls} = P \times (N_{CH})_{side-walls}$ on dielectric anode and side-walls, respectively. So, the number of PD pulses ($N_p$) which are required to convert all the existing epoxide rings to acid molecules may be obtained as follows:

$$(N_p)_{anode} = 2 \times (N_{DGEBA})_{anode} / (N_a)_{anode}  \qquad (13)$$
$$(N_p)_{side-walls} = 2 \times (N_{DGEBA})_{side-wall} / (N_a)_{side-walls}$$

The coefficient "2" is due to presence of two epoxide rings in each DGEBA monomer. Again, the number of cycles required to convert all epoxide groups to acid is as follows:

$$(N_{cycle})_{anode} = (N_p)_{anode} / N_{PDC}  \qquad (14)$$
$$(N_{cycle})_{side-walls} = (N_p)_{side-walls} / N_{PDC}$$

where $N_{PDC}$ indicates the number of PD pulses per cycle [4-7].

Hence, the time required to convert all epoxide rings to acid molecules at a supply

frequency of 50Hz (T=20ms) may be calculated as follows:

$$(t_c)_{anode} = T \times (N_{cycle})_{anode} \qquad (15)$$
$$(t_c)_{side-walls} = T \times (N_{cycle})_{side-walls}$$

where$t_c$ is the required time to convert all epoxide rings to acid molecules.

4. **Simulation Results**

In this paper, we present a typical simulation in which we trace the evolution of the distribution of charged particles within a narrow gas-filled channel. The simulation is performed with the chosen parameters presented in table II. It may be noted that a channel with a significantly large length / width ratio is chosen.

*Table II: Simulation data*

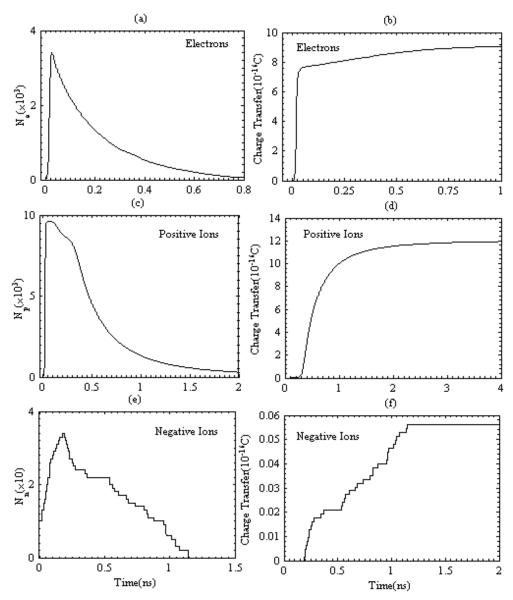| Property | Symbol | Value |
|---|---|---|
| Length of Narrow channel | $L_x$ | 20 μm |
| Width of Narrow Channel | $L_y$ | 1 μm |
| Depth of Narrow Channel | $L_z$ | 1 μm |
| Dielectric thickness | $L_d$ | 20 μm |
| Background gas pressure | $P_g$ | 101325 Pa |
| Background gas temperature | $T_g$ | 0.026 eV |
| External capacitor | C | 40 pF |
| Initial number of charged particles | $n_f$ | 10 |
| Photo-emission coefficient | $\lambda_{ph}$ | $5 \times 10^{-5}$ [38] |
| Ion-induced emission coefficient | $\lambda_i$ | $1.5 \times 10^{-3}$ [38] |
| Dielectric constant of air | $\varepsilon_0$ | $8.85 \times 10^{-12}$ F/m |

Figure 5: Time history of (a) number of electrons (b) transfer of electrons to the surrounding dielectric of the narrow channel, (c) number of positive ions (d) transfer of positive ions to the surrounding dielectric of the narrow channel, (e) number of negative ions (f) transfer of negative ions to the surrounding dielectric of the narrow channel.

Figure 5 shows the time history of number of electrons, positive and negative ions and charge transfer to dielectric anode and cathode associated with electrons and ions. The initial loading of electrons considered is sufficient for rapid ionization of the neutral gas molecules. It is observed that electrons leave the narrow channel very quickly (within 1ns), due to their higher mobility. Positive ions linger for almost 2 ns. Negative ions are depleted fast, within 1.2 ns. This is in agreement with simulation results obtained by Novak et al

using a fluid model and for a 0.5mm dielectric micro-gap [37].It may be noted that the total amount of charge transferred by the negative ions in a single pulse is $0.056\times10^{-16}$C, much lower than that due to migration of electrons ($9.027\times10^{-16}$C) and positive ions ($11.93\times10^{-16}$C). It is important to remember that any degradation in the channel is due to the sum total of the effects of numerous consecutive PD pulse.
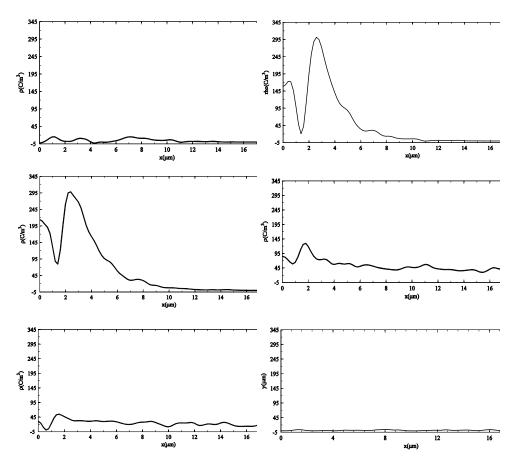


Figure 6: The net charge density spatial profile along the length of narrow channel for different configurations at $L_y$=0.5μm at different moments of time.

Figure 6 shows the variation of net charge density ($\rho=e(n_p-n_e-n_n)$) within the narrow channel with distance from the anode in the mid-width ($L_y$=0.5μm) at different instants of time. Where, $n_e$, $n_p$and$n_n$ are the densities of electrons, positive and negative ions. As observed for narrow cavities [37], the net charge density inside the narrow channel is mostly due to positive ions and net charge density decreases gradually towards the cathode. As seen in these figures, at the moments of 30ps and 90ps, in the region near the anode (x<2μm), the net charge density reaches very low values. This is the ionization

255

region, and before the charge particles drift towards the electrodes, the positive charge almost negates the effect of electrons, and the net charge density becomes very low. The very high positive value next to this region is the net charge density due to the large number of positively charged particles as they slowly drift towards the cathode. As time progresses, the positive ions move further and further away from the region of ionization towards the cathode and the peak in this region is reduced, the net charge density becoming more uniformly distributed along the inter-electrode distance. At t=2.4ns, most charged particles have left the narrow channel and net charge density is close to zero.
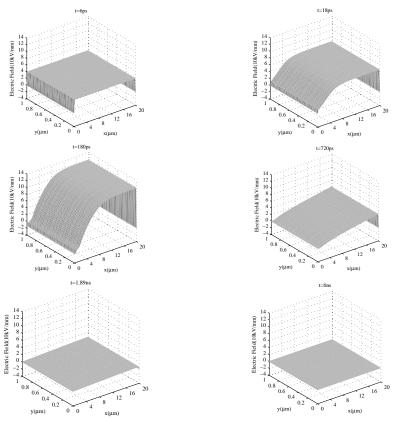


Figure 7: Spatial variations of x-component of electric field (Ex(x,y)) inside the narrow channel at different time moments.

The spatial variation of the x-component of electric field $(E_x(x,y))$ is depicted in figure 7. The distribution of field within the narrow channel is originally uniform. The distribution of charged particles inside the narrow channel (in figures 5 and 6) shows that the effect of space charge on applied field is mostly due to positive ions. A positive space charge region forms ahead of the anode where they accumulate. This results in a reduced field close to the anode. Simultaneously the field near the cathode is enhanced in the direction of the applied field, due to the positive charge cloud now nearing the negatively

charged cathode. Owing to the accumulation of negatively charged particles at the anode which causes the anode potential to reduce, the field at the anode never recovers original values. Finally, the field within the channel becomes uniform as the charge dissipates.
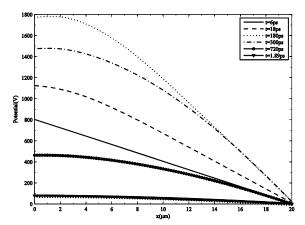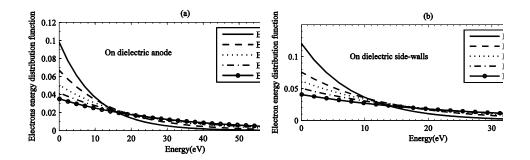


Figure 8: Variation of electric potential (V) along narrow channel length at different the different moments of time.

The spatial variations of electric potential (**E**=-**GradV**) across narrow channel at the different moments of time is presented in figure 8. The potential at t=6ps (almost at beginning of discharge) at x=0 (on dielectric anode) is around 800 V. Due to increased ionization, at the next time-steps the electric potential across the micro-cavity increases and finally comes back to its initial value. Due to the charge accumulation on the dielectrics, the electric potential never recovers its initial values.

Table III: Group composition of electrons ($N_{gk}$) impacting the dielectric anode at different applied electric fields.

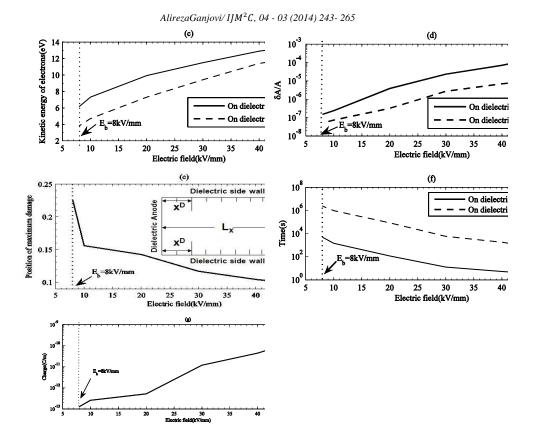| E(kV/mm) | $N_{g1}$ | $N_{g2}$ | $N_{g3}$ | $N_{g4}$ | $N_{g5}$ |
|---|---|---|---|---|---|
| 15 | 92 | 69 | 14 | 1 | 0 |
| 25 | 180 | 165 | 81 | 4 | 1 |
| 35 | 1810 | 892 | 444 | 93 | 5 |
| 45 | 2984 | 1283 | 796 | 271 | 25 |
| 55 | 5817 | 1741 | 1232 | 661 | 136 |

Figure 9: (a) EDF of electrons striking the dielectric anode surface, (b) EDF of electrons striking the surface of dielectric side walls, (c) average kinetic energy of electrons striking the dielectric anode and side walls, (d) variation of fractional area damaged ($\delta A/A$) during one PD pulse on dielectric anode and side-walls as a function of electric field across narrow channel, (e) distance (normalized) from dielectric anode of region of maximum damage ($x^D/L_x$) on dielectric side walls, (f) The time of conversion of entire of epoxide rings to acid molecules ($t_c$) on dielectric anode and side-walls as a function of electric field across narrow channel, (g) charge trapped to narrow channel side-walls during one single PD pulse as a function of electric field narrow channel.

As In this work, the material surrounding the dielectric narrow channel is assumed to be DGEBA. So, the presented results are confined to the issue of C-H bond scission due to electron impact.Table III shows the group composition of electrons ($N_{gk}$) impacting the dielectric anode at different applied electric fields. With higher electric fields, the total number of electrons reaching the dielectric anode is higher due to greater ionization. This matches the observation by Serra et al. [42] that the number of electrons generated inside a cavity increases with applied electric field. Also, understandably, increase in applied electric field results in larger proportion of hot electrons being produced.

Generally, the computation of the electron energy distribution functions (EEDF) of the electrons reaching the dielectric anode and side-walls could provide useful information

about PD pulse activity and the consequent damage into solid dielectric material.The energy distribution functions are helpful in understanding of the mechanism by which the highenergyelectronscan cause damage into solid dielectric materials due to PD activity within narrow channel.Figures 9(a) and 9(b) show that the Electron Energy Distribution Functions(EEDF's)are completely deviated from the Maxwellian distribution. These figures show that the increase in applied field is accompanied by a decrease in the proportion of cold electrons with energies less than 10eV. Then, the average value of electron temperature or kinetic energy of electrons at the dielectric anode increases with electric field (figure 9(c)). It means that the electrons acquire higher energies as they are accelerated in the stronger electric field within the narrow channel.

The combined effect of increased number of impacting electrons, and higher average energy of impacts, contribute to a higher number of C-H bond-scissions; a greater percentage of the dielectric anode surface is thereby degraded. As shown in figure 9(d), the effect of field on the extent of damage on the dielectric side-walls of the channel is similar to that on the dielectric anode. Kinetic energy, and therefore, degradation at the side walls increases at a steeper rate than at the dielectric anode, as a comparison of figures 9(c) and 9(d) shows.

A simple parametric fit on fractional area damaged ($\delta A/A$) for dielectric anode and side walls with electric field indicates a higher proportionality at the dielectric anode as given below:

$$\left(\frac{\delta A}{A}\right)_{\text{anode}} \propto (E)^{8.6} \qquad (16)$$
$$\left(\frac{\delta A}{A}\right)_{\text{side-wall}} \propto (E)^{6.75}$$

where $(\delta A/A)_{\text{anode}}$ and $(\delta A/A)_{\text{side-walls}}$ are respectively the fractional area damaged on dielectric anode and side-walls of tree channel. The quantity ($\delta A/A$) during one PD pulse is somewhat comparable to the "damage growth rate" of dielectric-void interface obtained by Montanari et al. [15, 30, 31, 42] in his aging model. Their estimation of the damage growth rate is based on the amount of energy dissipated in the insulating material surrounding a cavity, and obtained as the ratio of the thickness of the slab damaged ($D_{\text{dis}}$) to the total time ($t_{\text{dis}}$) required to dissociate at least half of the CH bonds inside this dielectric slab.

Interestingly, dielectric side-walls are not uniformly impacted by the damage-inducing electrons. The average distance at which the dielectric side-walls are struck is shown in Figure 9(e). As may be seen, regions very close to the anode (near 25% of the total channel length at lower electric fields of 8 kV/mm) are most damaged. The region of damage occurs closer the anode at higher applied electric fields for example, around 10% for

electric field with value of 50 kV/mm.

Figure 9(f) shows the effect of applied electric field on the time taken to convert all the epoxide rings on dielectric anode and side walls to acid molecules ($t_c$). The larger number of electrons and increased average kinetic energy of the electrons reaching the surrounding dielectrics (figure 9(c)), contribute to a reduction in the time for conversion of the epoxide rings on dielectric anode and side walls to acid molecules ($t_c$) in both cases. The time to conversion varies sharply with field, e.g. from 80 min to 2.53 s for dielectric anode, as the field increases from 8 kV/mm to 50 kV/mm. This would essentially mean an increased surface conductivity at higher electric fields, given the same time of exposure to discharge.

Two types discharge pulse forms, a spark-type and smaller Townsend have been reported [20-25] to occur within micro-channels. Kaminaga et al. reported that a free radical is generated in the initial phase of degradation of Polyethylene in high electric fields [26]. These free radicals are expected to react with oxygen and produce oxides, accompanied by luminescence. The number of free radicals was seen by them to increase with applied voltage [10-12].

As displayed in figure 9(f), theconversion time of the epoxide rings to acid molecules ($t_c$) varies from 666 h to 5.96 min for dielectric side-walls.The conversion time for dielectric side-walls is comparatively much higher than for dielectric anode. Conversion of all epoxide rings to acid molecules would cause an increase in surface conductivity of side-walls of tree tubule. It is reasonable to suppose that increased surface conductivity would lead to easy movement of charged particles along side walls and consequently a situation where no voltage can effectively be supported along the length of tree tubule; this might cause PD extinction. Dissado et al. [15, 16] reported that movement of charges on the tubule wall can short-circuit a discharge.

In this paper, we see that the time required for conversion of dielectric side-walls to conductive walls is two orders of magnitude greater than the time needed for the dielectric anode. This indicates that it might be expected that after a sufficient number of spark-type pulses, there would be a change in the nature of the discharge i. e. from pulse-type to glow. It is therefore unlikely that the discharge along a tree tubule would be extinguished with time; rather a transition in the nature of the discharge is likely to occur. This corroborates the results by Hudon et al. who reported the occurrence of glow discharges at very long times [20, 21].

The effect of applied electric field on the magnitude of trapped charge on the dielectric side-walls of the tree channel during one PD pulse is depicted in figure 9(g). A larger number of charges (mostly electrons) reaches the dielectric side-walls at higher fields.

260

Auckland et al [1, 3] confirmed that avalanches within the gas-filled channel generate charges which are deposited on the walls or are trapped within the solid, reducing the voltage across the channel and extinguishing further avalanches. The initial luminosity of the breakdown originates within the solid, before a visible discharge occurs in the gas. Finally, increase in applied electric field increases ionization and the number of impacts per discharge and, as a result tends to cause greater cumulative damage over time as well as increase in surface conductivity. At higher fields, the increased degradation is due to an increase in the number of impacting charged particles, in spite of decrease in average impact energy. The time required to convert tree side-walls to a conductive surface ($t_c$) is much longer compared to that required for dielectric anode, and this is true for all values of electric field. This means that the transition from spark to glow discharges occurs at smaller time-scales than discharge extinction at all values of electric field. While increased number of impacts is accompanied by a decrease in the average energy at the impact site, the amount of charge deposited to surrounding dielectrics increases.

### 4. **Conclusions**

A Kinetic model based on a 2-dimensional PIC-MCC scheme has been successfully used to study of a PD activity inside a dielectric narrow channel. The model successfully yields detailed information about effect of applied electric field on the damage due to partial discharges activity into surrounding dielectrics of a narrow channel encapsulated within the volume of a dielectric material.

It is seen that the charged particles accumulation causes the development of an induced electric field by space charges that opposes the applied electric field. Computation of energy distribution functions of the electrons reaching the dielectric anode and side-wallsfor electric field values is one of the most important contributions of this work.

The obtained results showed that the Energy Distribution Functions (EDF) of the striking electrons onto the dielectric anode and side-walls is completely deviated from the Maxwellian distribution, and by increasing of the applied electric field,the proportion of cold electrons decreases.

The damage to the dielectric anode and side-walls in terms of C-H bond scission as well as increase in conductivity due to formation of acid droplets is estimated. The effect of the discharge on the surrounding dielectrics is such as to favor a change in the nature of the discharge rather than to lead to discharge extinction.

**Appendix**

261

The total charge density $\sigma_T$ on the anode metallic electrode may be expressed by [48]:

$$\sigma_T^t = \sum_{j=0}^{N-1} \sigma_{0j}^t \quad (A1)$$

where $\sigma_{0j}^t$ is the surface charge density on anode electrode at time 't'. The simplified form

of equation (26) of [48] for a 'simple metallic-metallic' configuration (ref. [19]) is:

$$\sigma_T^t = \frac{\varepsilon_0}{\Delta x} N\phi_0^t - \frac{\varepsilon_0}{\Delta x} \sum_{j=0}^{N-1} \phi_{1j}^t - \frac{\Delta x}{2} \sum_{j=0}^{N-1} \rho_{0j} \quad (A2)$$

where, $\phi_0^t$, $\phi_{1j}^t$, N are the potential on the anode at 't', potential at $x_1(=1\times\Delta x)$ and number of

divisions along y-axis. Particle 'p' contributes to $Q_{ij}$ through the space charge density $\rho_{ij}$

(bilinear weighting: [48]).

The equivalent circuit for the narrow channel bounded by dielectrics is shown in figure

2(b). $C_g$, $C_d$ and $C_r$ represent the equivalent capacitances of the gap, the dielectric layers

and dielectric material parallel to the micro-channel respectively, and $J_{conv}$ is the discharge

current density. The time variation of $\sigma_T$, the total charge density on the driven dielectric

electrode, may be obtained from the Kirchhoff 's Current Law:

$$A\frac{d\sigma_s}{dt} = I_{ext} - I_r + AJ_{conv}, \quad (A4)$$

where $I_{ext}$, $\sigma_T$ and $I_r$ the total external current, charge on the dielectric surfaces and current

in the dielectric material parallel to the narrow channel.

The time variation of voltage drop ($U_d$) across the dielectric slab is obtained as:

$$C_d\frac{dU_d}{dt} = I_{ext} - I_r \cdot \quad (A5)$$

Figure 2(b) shows a simple external circuit consisting of a voltage source in series with

a capacitor coupled to the left electrode. The voltage drop $V_c$ across the capacitor in the

external circuit is obtained from voltage balance as,

$$V_c = V(t) - 2U_d - \phi_0 \quad (A6)$$

V(t) is the applied voltage source. The discrete finite differenced form of (A4) can be

expressed as:

$$A(\sigma_T^t - \sigma_T^{t-1}) = Q_c^t - Q_c^{t-1} - Q_r^t + Q_r^{t-1} + Q_{conv}^t \quad (A7)$$

where $\int I dt = Q_c = CV_c$ and $\int I_r dt = Q_r = CU_r$ and are the charge on the external capacitor

and bulk of dielectric material parallel to the narrow channel, and $Q_{conv}^t$ is the charge

deposited on the electrode from the discharge in the cavity during the time interval (t-1, t).

Combining equations (A6) and (A7), the following relation can be obtained:

$$\sigma_T^t = \sigma_T^{t-1} + \frac{1}{A}(CV(t) - (C+C_r)\varphi_0^t - 2(C+C_r)U_d^t + Q_r^{t-1} - Q_c^{t-1} + Q_{conv}^t)(A8)$$

Similarly, the discrete finite differenced form of (A5) can be expressed as:

$$U_d^t - U_d^{t-1} = \frac{1}{C_d}\int (I_{ext} - I_r)dt = \frac{Q_c^t - Q_c^{t-1} - Q_r^t + Q_r^{t-1}}{C_d} \text{ (A9)}$$

If equations (A6) and (A9) are combined, then we have:

$$U_d^t = \frac{U_d^{t-1} + \frac{1}{C_d}(CV(t) - (C+C_r)\varphi_0^t - Q_c^{t-1} + Q_r^{t-1})}{1+(C+C_r)/C_d} \text{ (A10)}$$

By inserting the value of $U_d^t$ to the equation (A8) and taking $\alpha=(1+2(C+C_r)/C_d)^{-1}$, the value of $\sigma_T^t$ can be written as follow:

$$\sigma_T^t = \sigma_T^{t-1} + \frac{1}{A}(\alpha CV(t) - \alpha(C+C_r)\varphi_0^t - 2\alpha(C+C_r)U_d^{t-1} - \alpha Q_c^{t-1} + \alpha Q_r^{t-1} + Q_{conv}^t). \quad \text{(A11)}$$

Equations (A1), (A2) for $\sigma_T^t$ and (A11) can be combined and solved for $\phi_0^t$ on dielectric anode to produce:

$$\phi_0^t = (\sigma_{s_T}^{t-1} + \frac{1}{A}(\alpha CV(t) - \alpha Q_c^{t-1} + \alpha Q_r^{t-1} - 2\alpha(C+C_r)U_d^{t-1} + Q_{Conv}^t) + \frac{\Delta x}{2}\sum_{j=0}^{j=N}\rho_{0j} + \frac{\varepsilon}{\Delta x}\sum_{j=0}^{j=N}\phi_{1j}^t)(\frac{\varepsilon}{\Delta x}N + \alpha(C+C_r)/A)^{-1}$$

(A12)

## Acknowledgment

## References

[1]    Auckland D. W., Borishade A. B., and Cooper R., *Photographic investigation of breakdown of composite insulation*, Proceedings of IEE, **124(12)** (1997) 1263-1266.

[2]    Auckland D. W., Borishade A. B., and Cooper R., *The breakdown characteristics of air-filled tubules in solid insulation*, IEEE Conference Publication, Dielectric Materials, Measurements and Applications, Cambridge,(1975) 15-18.

[3]    Auckland D. W., Kabir S. M. F and Varlow B. R., *Charge deposition in gas filled channels with insulating walls*, IEE proceedings-A, **140(6)** (1993) 509-516.

[4]    Bartnikas R., *Discharge rate and energy loss in helium at low frequencies*, Electrical Engineering, **52** (1969) 348-359.

[5]    Bartnikas R., Engineering Dielectrics, Vol. I, *Corona Measurement and Interpretation*, R. Bartnikas and E. I. McMahon, Editors, SlT669, ASTM, Philadelphia, (1979).

[6]    Bartnikas R., *Note on ac discharges between metallic-dielectric electrodes in helium*, Journal of Applied Physics, **40** (1969) 1974-1976.

[7]    Bartnikas R., *Some observations on the character of corona discharges in short gap spaces*, IEEE Transactions on Electrical Insulation,**6(2)** (1971) 63-75.

[8]    Birdsall C. K. and Langdon A. B., *Plasma physics via computer simulation*, McGraw-Hill, New York, (1985).

[9]    Birdsall C. K., *Particle-in-cell charged-particle simulations, plus Monte Carlo collisions with neutral atoms, PIC–MCC*, IEEE Transactions on Plasma Science, **19** (1995) 65–85.

[10]   Blythe A. R., Briggs D., Kendall C. R., Rance D. G. and Ziehy V. J. I, *Surface modification of polyethylene by electrical discharge treatment and the mechanism of autoadhesion*, Polymer, **19** (1978) 1273-1278.

[11]   Briggs D. and Kendall C. R., *Chemical basis of adhesion to electrical discharge treated polyethylene*, Polymer, **20** (1979) 1053-1054.

[12]   Briggs D. and Kendall C. R., *Derivation of discharge-treated LDPE: an extension of XPS analysis and a probe of specific interactions in adhesion*, Int.   Journal of Adhesion and Adhesive, (1982) 13-17.

[13]   Briggs D., Blythe A. R., Kendall C. R. and Wootton A. B., *Electrical discharge treatment of polypropylene film*, Polymer, **24** (1983) 47-52.

[14] Briggs D., Blythe A. R.,Kendall C. R. and Rance D. G.,*Surface modification of poly (ethylene terephthalate) by electrical discharge treatment*, Polymer, **21** (1980) 895-900.

[15] Dissado L. A., Mazzanti G. and Montanari G. C., *Propagation of electrical tree structures in solid polymeric insulation*, IEEE Transactions on Dielectrics and Electrical Insulation,**4(5)** (1997) 496-596.

[16] Dissado L. A., Mazzanti G. and Montanari G. C., *The role of trapped space charges in the electrical aging of insulating materials,* IEEE Transactions on Dielectrics and Electrical Insulation,**4(5)** (1997) 496-596.

[17] *FariborziAraghi M. A. and MamizadehChatghayeh S., The Use of a Runge-Kutta Scheme for an ODE-PDE Model of Supply Chains*, International Journal of Mathematical Modeling & Computations, **3(1)** (2003) 43-50.

[18] Gamez-Garcia M., Bartnikas R. and Wertheimer M. R, *Synthesis reactions involving XLPE subjected to partial discharges*, IEEE Transactions on Electrical Insulation, **EI-22(2)** (1987) 199-205.

[19] Ganjovi A. A., Gupta N. and Raju G. R. G., *A kinetic model of a PD pulse within voids of sub-millimeter dimensions*, IEEE Transactions on Dielectrics and Electrical Insulation,**16(6)** (2009) 1743-1754.

[20] Hudon C. and Bartnikas R., *Surface conductivity and gas phase reactions arising with epoxy exposed to partial discharges*, IEEE Conference on Electrical Insulation and Dielectric Phenomena, (1992) 725-34.

[21] Hudon C., Bartnikas R. and Wertheimer M.R., *Chemical and physical degradation effects on epoxy surfaces exposed to partial discharges*, 4th International Conference on Properties and Applications of Dielectric Materials, Brisbane Australia, (1994) 811-814.

[22] Hudon C., Bartnikas R. and Wertheimer M.R., *Effect of physico-chemical degradation of epoxy resin on partial discharge behavior*, IEEE Transactions on Dielectrics and Electrical Insulation, **2(6)** (1995) 1083-1094.

[23] Hudon C., Bartnikas R. and Wertheimer M.R., *Spark-to-glow discharge transition due to increased surface conductivity on epoxy resin specimens*, IEEE Transactions on Dielectrics and Electrical Insulation, **28(1)**(1993) 1-8.

[24] Hudon C., Bartnikas R. and Wertheimer M.R., *Surface conductivity of epoxy specimens subjected to partial discharges*, IEEE International Symposium on Electrical Insulation, Toronto, Canada, (1990) 3-6.

[25] Ishida T., Kosaki M., Mizuno Y. and Nagao M.,*Computer aided partial discharge analyzing system for detection of swarming pulsivemicrodischarges*, IEE Conference Publication, (1993) 99-100.

[26] Kaminaga K., Fukui T., Haga T., Suzuki T., Uozumi T. and Yasuda N.,*The mechanism of degradation of polyethylene in a high electrical field*, Conference on Electrical Insulation and Dielectric Phenomena, (1993) 666-71.

[27] Lawson W. S., *Particle simulation of bounded 1D plasma systems*, Journal of Computational Physics, **80** (1989) 253-276.

[28] Mardahl P. J. and Cartwright K. L., *Reducing numerical heating in 1-D PIC simulations*, Annual Progress Report for 1993, Plasma Theory and Simulation Group, University of California Technical Memorandum, Electronics Research Laboratory, Berkeley, (1993).

[29] Mardahl P. J., and Verboncoeur J. P., *Charge conservation in electromagnetic PIC codes; spectral comparison of Boris/DADI and Langdon-Marder methods*, Computer Physics Communications, 106 (1997) 219-229.

[30] Mayoux C., Garcia G. and Sarlaboux J., *Interaction of corona with dielectric material until damage*, IEEE Transactions on Electrical Insulation, **EI-17(2)** (1982) 156-162.

[31] Mazzanti G.,Civenni F. and Montanari G. C, *Model of inception and growth of damage from microvoids in polyethylene-based materials for HVDC cables part 2: parametric investigation and data fitting*, IEEE Transactions on Dielectrics and Electrical Insulation, **14(5)** (2007) 1255-1263.

[32] Mazzanti G.,Civenni F. and Montanari G. C.,*Model of inception and growth of damage from microvoids in polyethylene-based materials for HVDC cables part 1: theoretical approach*, IEEE Transactions on Dielectrics and Electrical Insulation, **14(5)** (2007) 1242-1254.

[33] McMahon E. J. and Perkins J. R., *Surface and volume phenomena in dielectric breakdown of polyethylene*, IEEE Transactions on Plasma Science, **82(69)** (1963) 1128-1136.

[34] *Mirshojaei S. S., Fayazzadeh S., The Comparison of Efficient Radial Basis Functions Collocation Methods for Numerical Solution of the Parabolic PDE's*, International Journal of Mathematical Modeling & Computations, **1(2)** 2011 60-73

[35] Morshuis P. H. F. and Kreuger F. H., *The spatial distribution and electrical parameters of partial discharges in polyethylene insulation during aging*, Proc. 4th Int. Conf. Cond. Breakd. Solid Dielectrics, SestriLevante/Italy, (1992) 209-214.

[36] Morshuis P. H. F. and Kreuger F. H., *Transition from streamer to Townsend mechanisms in dielectric voids*, Journal of Physics D: Applied Physics, **23** (1990) 1562-1568.

[37] Novak J. P and Bartnikas R., *Quantitative model of a short-gap breakdown in air, XVIIth International symposium on discharge and electrical insulation in vacuum*, Berkeley, (1996) 60-64.

[38] Novak J. P. and Bartnikas R., *Ionization and excitation behavior in a micro-cavity*, IEEE Transactions on Dielectrics and Electrical Insulation, **2(5)** 1995 724-728.

[39] Raju G. R. G., *Gaseous Electronics: Theory and Practice*, Boca Raton,. FL: Taylor and Francis (2005).

[40] Rogers E. C, Grad E. B. and Harriss V. G., *A servo-mechanism for the study of self-extinction of gaseous discharges in cavities in dielectrics*, Journal of Scientific Instrumentation, **33** (1956) 7-10.

[41] Roldan A., Blanco F. Garcia G., Perez J. M. and Williart A., *Energy deposition model for low-energy electrons (10-10 000 eV) in air,*Journalof Applied Physics, **95(10)** (2004) 5865-5870.

[42] Serra S., Mazzanti M. and Montanari G. C., *Theory of inception mechanism and growth of defect-induced damage in polyethylene cable insulation*, Journal of Applied Physics, **98** (2005) 034102-1-15.

[43] Shimizu N. and Laurent C., *Electrical tree initiation*, IEEE Transactions on Dielectrics and Electrical Insulation, **5(5)** (1998) 651-659.

[44] Tanaka T. and Ikeda Y., *Internal discharges in polyethylene with an artificial cavity*, IEEE Transactions on Plasma Science, **PAS-90(6)** (1971) 2692-2702.

[45] Theodorou, D.N., Understanding and predicting structure property relations in polymeric materials through molecular simulations. *Molecular Physics*. **102** (2004) 147-166.

[46] Vahedi V. and DiPeso G., *Simultaneous Potential and Circuit Solution for Two-Dimensional Bounded Plasma Simulation Codes,* Journal of Computational Physics, **131** (1997) 149-163.

[47] Vahedi V. and Surendra M., *Monte-Carlo collision model for particle-in-cell method: application to argon and oxygen discharges*, Computer Physics Communications, **87** (1995) 179–98.

[48] Vahedi V., Birdsall C. K., DiPeso G., Lieberman M. A. and Rognlien T. D., *Verification of frequency scaling laws for capacitive radio-frequency discharges using two-dimensional simulations*, Physics Fluids B, **5** (1993) 2719-2729.

[49] Verboncoeur J. P., *Symmetric spline weighting for charge and current density in particle simulation*, Journal of Computational Physics, **174** (1997) 421-427.

[50] Wolter K. D., Tanaka J., and Johnson J. F., *A study of the gaseous degradation products of corona-exposed polyethylene*, IEEE Transactions on Electrical Insulation, **E1-17(3)** (1982) 248-252.

[51] Zhang W., Fisher T. S. and Garimella S. V., *Simulation of ion generation and breakdown in atmospheric air*, Journal of Applied Physics, **96**(2004) 6066-6072.